# Evaluation of the Behavior of Equal and Variable-Length Piles in Soft Clay Using Field Load Tests and Finite Element Modeling

**Lan V. H. Bach**
Faculty of Civil Engineering, University of Architecture, Ho Chi Minh City, Vietnam
lan.bachvuhoang@uah.edu.vn (corresponding author)

*Received: 4 September 2025 | Revised: 22 September 2025 and 8 October 2025 | Accepted: 12 October 2025*

 *DOI: https://doi.org/10.48084/etasr.14525*

## ABSTRACT

**This study examines the performance of Equal-Length (EL) and Variable-Length (VL) pile groups with rigid caps under central axial loads, focusing on load-bearing capacity, load distribution, and unit shaft resistance. Small-scale loading tests are performed on both groups. The EL group consists of steel pipe piles, 60 mm in diameter and 1,800 mm long, while the piles in the VL group are estimated using Feld's rule to maintain a consistent total length between the groups. The Finite Element Method (FEM) is also used to validate the results, based on real pile groups driven in Saigon South, District 7, Ho Chi Minh City, Vietnam. The small-scale field test results show that the VL pile group achieved nearly 20% higher bearing capacity compared to the EL pile group of the same size and total pile length. The data indicate that load distribution in the EL pile group was considerably uneven, with the load on the corner pile being roughly 10% higher than on the edge pile and 31% higher than on the center pile. Conversely, the VL pile group demonstrated a more even load-distribution, with differences between piles not exceeding 10%. The FEM supported these trends, confirming the model's accuracy in predicting load-sharing effects in complex pile arrangements and reinforcing the structural advantages of VL configurations. Additionally, the VL pile group method provides cost savings by reducing material requirements and construction time compared to traditional EL pile foundations. These findings highlight the potential of VL pile groups as a cost-effective, high-performance solution for centric load foundations in challenging soil conditions, offering improved load-bearing capacity, balanced load-distribution, and reduced construction costs.**

***Keywords-load distribution; variable-length pile group; equal-length pile group; load-settlement behavior; static load testing***

## I. INTRODUCTION

Raft foundation designs often struggle to effectively control both total and differential settlements, especially under heavy loads and Soft Soil (SS) conditions. Therefore, piled raft foundations combine a raft that distributes the superstructure loads with piles that are designed to bear these loads [1, 2]. These piled rafts are engineered to ensure stability in SS environments. The raft in a piled raft is typically designed to be rigid enough to evenly distribute loads to each pile, thereby eliminating differential settlement. To achieve this, various pile configurations beneath the raft have been proposed. Increasing raft rigidity results in a more even load distribution among the piles [3, 4]. Consequently, the loads at the top of each pile vary, necessitating different pile design lengths.

In practice, piles in piled raft foundations are usually designed with uniform lengths, which simplifies construction but often causes uneven load distribution, leading to different settlements among the piles. Meeting consistent settlement requirements in such systems may require using piles of different lengths or modifying pile configurations, both of which can increase construction costs and extend project timelines. Therefore, researchers use VL piles within a single foundation system to optimize both capacity and settlement control [5-7]. Optimization analyses indicate that pile groups with variable lengths improve load-bearing efficiency and reduce settlement in soft clay foundations. Authors in [8] analyzed several case studies on foundations with VL piles in soft clay conditions. They recognized that customized pile lengths based on external loads can improve load distribution and significantly decrease overall foundation settlement. Authors in [9] presented an approach that utilizes the interaction between piled raft and soil to create an optimal design that meets both serviceability and ultimate limit states. They investigated VL piles in pile raft foundations designed explicitly for soft clay, which reduced differential settlement and enhanced foundation performance. According to the optimization theory, pile groups with rigid caps can ensure equal load distribution on pile heads and minimize both the total and differential movements of the foundation [10]. Using the Modified Unified Method to calculate loads, authors in [11, 12] optimized each pile length by considering bearing capacity, settlement, and negative friction simultaneously. However,

most of these studies are theoretical; few investigations are based on real-world application models.

This study employs small-scale field load testing and finite element modeling to evaluate the performance of EL and VL pile groups under rigid caps in SS conditions in Ho Chi Minh City, Vietnam. The assessment focuses on the mobilized pile bearing capacity, pile head load, total settlement, and differential settlement of the two pile foundation models.

## II. MATERIALS AND METHODS

### A. Subsoil Conditions

The field testing was conducted at a site in the Saigon South area, District 7, Ho Chi Minh City, Vietnam, where the subsoil consists of a thick layer of soft, normally consolidated, compressible clay. The natural water table is approximately 1.0 m below the ground surface, and the clay layer extends to a depth of about 30.5 m. Beneath this, medium to stiff, green-grey clay is found at a depth of around 41.7 m. The average saturated density of the soft clay is approximately 1,490 kg/m³. More details of the soil properties are shown in Table I.

TABLE I. MATERIAL PROPERTIES OF CLAY SOIL LAYER

| Parameter | Symbol | Value | Unit |
|---|---|---|---|
| Unit weight above the phreatic level | $\gamma_{unsat}$ | 14.9 | kN/m$^3$ |
| Unit weight below the phreatic level | $\gamma_{sat}$ | 15.1 | kN/m$^3$ |
| Initial void ratio | $e_{init}$ | 2.149 | - |
| Cohesion | $c'_{ref}$ | 8.6 | kN/m$^2$ |
| Friction angle | $\varphi$ | 2.7 | degrees |
| Dilatancy angle | $\psi$ | 0 | degrees |
| Modified compression index | $\lambda^*$ | 0.096 | - |
| Modified swelling index | $\kappa^*$ | 0.021 | - |
| Poisson's ratio for unloading/ reloading | $v_{ur}$ | 0.15 | - |
| Coefficient of lateral stress in normal consolidation | $K_{0nc}$ | 0.95 | - |
| Coefficient of horizontal permeability | $k_x = k_y$ | 7.38E-8 | m/day |
| Coefficient of vertical permeability | $k_z$ | 1.84E-8 | m/day |
| Interface strength reduction (clay/steel) | $R_{inter}$ | 0.5 | - |

### B. Small-Scale Field Load Tests

#### 1) Pile Group Simulation

The layouts of two pile groups and the rigid cap of the 16-pile group are displayed in Figure 1.

Each pile was made from steel pipes with an outer diameter (D) of 60 mm and an inner diameter of 50 mm. The steel pile material has an elastic modulus of E=225 GPa. Both pile groups were arranged in a square pattern, with a steel rigid cap placed above each group to transmit the applied load directly to the pile group. The pile heads were embedded in the ground surface about 0.5 m. This setup allows a focused investigation of how axial loads are transferred through the piles alone, without interference from raft–soil interaction.

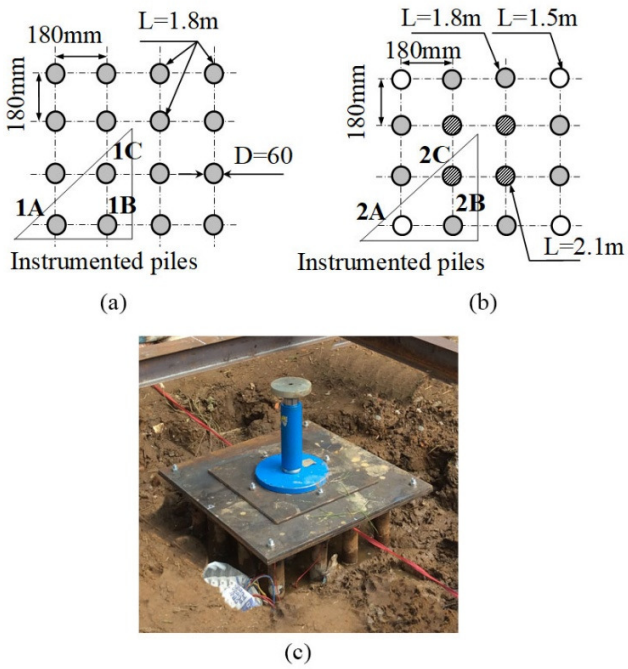


Fig. 1. Layouts of two pile groups: (a) EL pile group with lengths 30D=1.8m, (b) different-length/VL pile group with lengths 1.5m-2.1m, (c) the position of the 16-pile group with a rigid cap.

A center-to-center pile spacing of 0.18 m (approximately three times the pile diameter) was used to match the small-scale model and investigate pile load distribution, ensuring that all 16 piles fit within the test footprint. The pile lengths of the two groups are:

- For the EL pile group, all piles were driven to a depth of 1.8 m, which is 30 times the pile diameter, to ensure the slenderness ratio.
- For the the VL pile group, the piles were arranged with varying lengths.

Three piles in each group were equipped with strain gauges to measure deformation during testing. Each test pile had one gauge level placed above the ground surface (GL0) and 2-4 additional gauge levels installed below ground, as depicted in Figure 2, specifically:

- For the 1.5 m piles (GL1 and GL2), strain gauges were installed at depths of 0.6 m and 1.5 m.
- For the 1.8 m piles (GL3), an additional gauge was added at the level of 1.8 m.
- For the 2.1 m piles (GL3 and GL4), two additional gauges were installed at levels 1.8 m and 2.1 m.

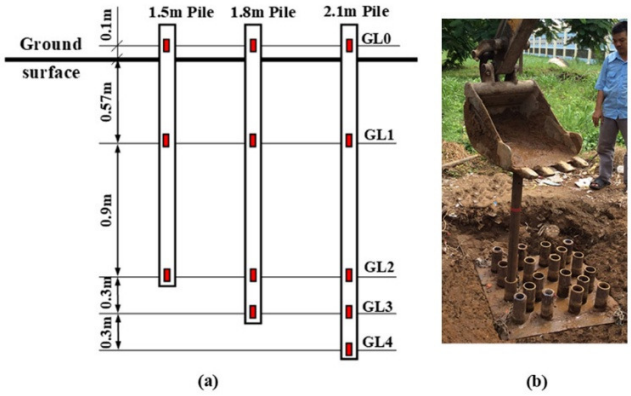


Fig. 2. Positioning strain gauges on piles and the pile press-in process: (a) the strain gage levels on the instrument piles, (b) the installation of the piles.

Axial strains were measured using foil strain gauges (KYOWA KFG-1-120-C1-11L1M2R) with a range of ±5,000 με and an accuracy of ±0.5% full scale. The gauges were connected to a National Instruments DAQ-9172 chassis equipped with NI 9237 bridge modules, recording at 10 Hz.

*2) Estimate Pile Lengths for Variable-Length Pile Group*

To determine the optimal pile lengths in the VL pile group, Feld's rule [13] was used to account for group effects. According to this method, each pile's bearing capacity is decreased by the presence of neighboring piles, as follows:

- Corner piles are reduced by three-sixteenths (3/16)
- Edge piles are reduced by five-sixteenths (5/16)
- Center piles are reduced by one-half (1/2)

The efficiency of the pile group ($\eta$) was calculated as the average efficiency across all piles, using:

$$\eta = \frac{(e_C \times n_C) + (e_S \times n_S) + (e_{CE} \times n_{CE})}{n_C + n_S + n_{CE}} \quad (1)$$

where $n_C$, $n_S$, and $n_{CE}$ are the number of corner, side, and center piles, respectively, and $e_C$, $e_S$, and $e_{CE}$ represent the efficiencies of each pile type.

The proportion of the load distributed on the pile head diminishes in the following order: corner piles, edge piles, and center piles within the group. Utilizing this formula, the load distribution ratio per pile ($p_i$) was calculated using (2) to assist in determining the optimal pile lengths for the load balancing group:

$$p_i = \frac{e_i}{n_i} \quad (2)$$

where $\eta$ is the efficiency of a pile group and $e_i$ is the efficiency of each pile position in a pile group.

To simplify the design of the VL pile group, several assumptions were made:

- The bearing capacity of each pile in the group is directly proportional to its length.
- The total pile lengths of the 16 piles in both the EL and VL groups are the same.

Based on these assumptions and the load distribution ratio per pile ($p_i$), the calculated lengths for each pile position are portrayed in Table II. However, for ease of manufacturing, the pile lengths used were: corner piles were 1.5 m (L/D=25), edge piles were 1.8 m (L/D=30), and center piles were 2.1 m (L/D=35).

TABLE II. ESTIMATED LENGTHS OF THE VL PILE GROUP

| Type of pile | Number of piles | Pile efficiency | Group efficiency | Load distribution ratio per pile | Length |
|---|---|---|---|---|---|
| | $n_i$ | $e_i$ | $\eta$ | $p_i$ | $l_i$ |
| Corner | 4 | 0.8 | 0.67 | 1.19 | 2.14 |
| Edge | 8 | 0.69 | | 1.02 | 1.80 |
| Center | 4 | 0.5 | | 0.75 | 1.46 |

*3) Static Load Testing Procedure*

The static load tests were performed following the quick load test procedure to minimize the errors caused by creeping effects [14, 15]. For the EL pile group, testing was carried out in two cycles.

- Cycle 1: Conducted in 12 incremental loading steps, reaching a maximum load of approximately 24 kN, followed by unloading in 6 steps.
- Cycle 2: Included 10 incremental loading steps, reaching failure at approximately 40.2 kN, with similar unloading steps.

Turning to the VL pile group, the test involved a single loading cycle with 12 increments, each increasing by 4 kN, followed by unloading in the same steps. The field tests are conducted using apparatus mounted on the rigid caps, as shown in Figure 3. All data were recorded at each increment to analyze the performances of the two pile groups.

Fig. 3. Setup of the measuring apparatus on the test pile group to record the loads, movements, and deformation of each instrumented pile.

## *C. Finite Element Method*

FEM was employed to simulate the behavior of pile groups in soft clay under static loads. Utilizing Plaxis 3D software [16], a FEM model was developed to replicate the

configurations and load conditions observed in field tests, facilitating a comparison between EL and VL pile groups, as displayed in Figure 4.

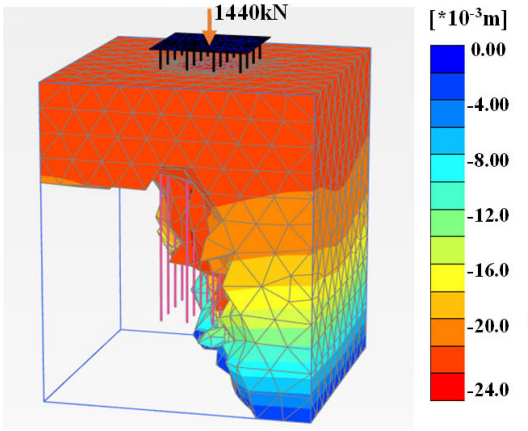


Fig. 4. Modeling of the two pile groups at the last load levels: (a) EL pile group, (b) VL pile group.

### *1) Pile Group Simulation*

In the FEM model, the pile groups were scaled up to full size, with all piles modeled as hollow circular sections. Each pile had an outer diameter of 400 mm and an inner diameter of 330 mm. The center-to-center spacing between piles in both groups was set at three times the pile diameter.

- EL Pile Group: All piles were embedded to a depth of 12 m ($L/D$=30).
- VL Pile Group: The piles in this group were embedded at varying depths—10 m for corner piles, 12 m for edge piles, and 14 m for center piles.

The installation of piles was simplified through the utilization of the "wished-in-place" method, and explicitly, no excess pressure buildup or setup effect was modeled.

### *2) Soil and Pile Simulation*

The soil was simulated using the SS model, which was designed to simulate the compressibility and normally consolidated behavior of the clay. The material properties for the pile raft and steel piles used in the FEM model are illustrated in Table III.

TABLE III. MATERIAL PROPERTIES OF RAFT AND PILES

| Parameter | Unit | Symbol | Pile | Raft |
|---|---|---|---|---|
| Type of behavior | - | - | Elastic | Linear, isotropic |
| Pile type | - | - | Predefined | - |
| Shape | - | - | Circular hollow | Plate |
| Diameter | m | dpile | 0.4 | - |
| Thickness | m | - | 0.0125 | 0.2 |
| Young's modulus | kN/m$^2$ | E | 225.106 | 225.106 |
| Unit weight | kN/m$^3$ | γ | 78.5 | 78.5 |
| Axial skin resistance | - | - | Linear | - |
| Maximum skin resistance allowed at the top of the embedded pile | kN/m | Tskin, start, max | 5 | - |
| Maximum skin resistance allowed at the bottom of the embedded pile | kN/m | Tskin, end, max | 10 | - |
| Maximum base resistance allowed | kN | Fmax | 50 | - |

## III. RESULTS AND DISCUSSION

### *A. Results Obtained by Field Tests*

A comparison of the static load test results for the two pile groups is presented in Figure 5. As the load increases, both pile groups shift from linear to nonlinear behavior. However, the VL pile group enters this nonlinear phase at a larger load. Regarding the test results, the EL pile group reaches its maximum load capacity at about 40 kN, with a settlement of 18.5 mm. In contrast, the VL pile group withstands a higher peak load of approximately 48 kN at a settlement of 17.4 mm. Research indicates that VL pile groups provide roughly 20% greater load capacity compared to EL pile groups.

The minor residual deformation observed in the VL pile group indicates that, while it effectively enhances load-bearing capacity, this setup influences load distribution and results in differential responses among the piles [17, 18].

Figure 6 portrays a comparison of strain gauge readings at the pile head (GL0) for each pile in the two groups. This gauge level indicates the maximum deformation for each pile. The highest strain recorded was 16 μ in Pile 2B. The strains in Pile 2B and Pile 2C of the VL pile group exceeded those in the first group, indicating a higher load distribution on these piles.

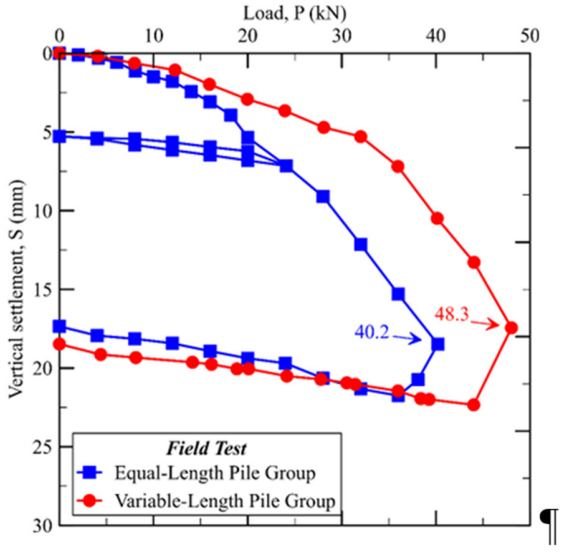


Fig. 5. Load-settlement curves of two pile groups (field tests)

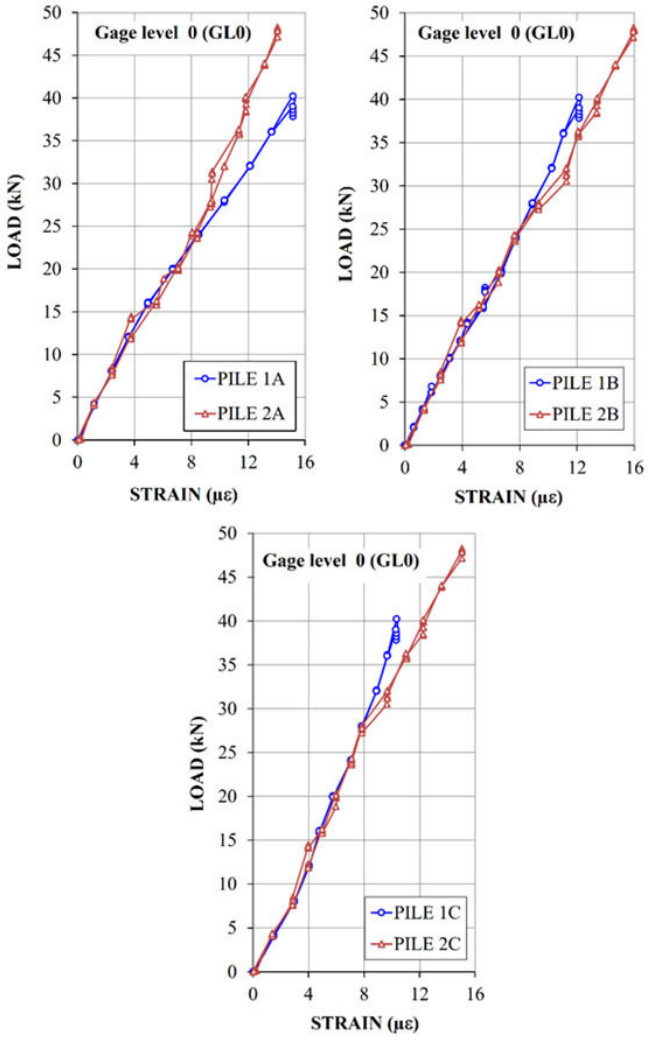


Fig. 6. Load-strain curves at gage level 0 (GL0) of the two pile groups.

## B. Results Obtained by the Finite Element Method

The load-settlement curves for both pile groups obtained by FEM (Figure 7) show the transition to collapsing failure, identified by a significant change in slope. The EL pile group fails at approximately 1,320 kN, while the other group withstands a higher failure load of about 1,680 kN. The load capacity increases by around 24,5% for the VL configuration. At maximum load, the vertical displacements of the EL and VL pile groups are 14.5 mm and 13.9 mm, respectively.

Figure 8 shows the axial force ($N_z$) distribution in the piles for both groups at their failure load. The axial forces decrease with depth due to frictional forces between the pile surface and the surrounding soil. The VL pile configuration distributes forces differently, which may help increase load capacity by balancing frictional resistance more effectively.

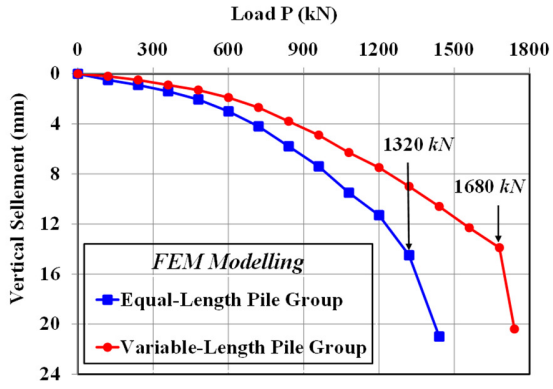


Fig. 7. The load-settlement behavior of the two pile groups (FEM).

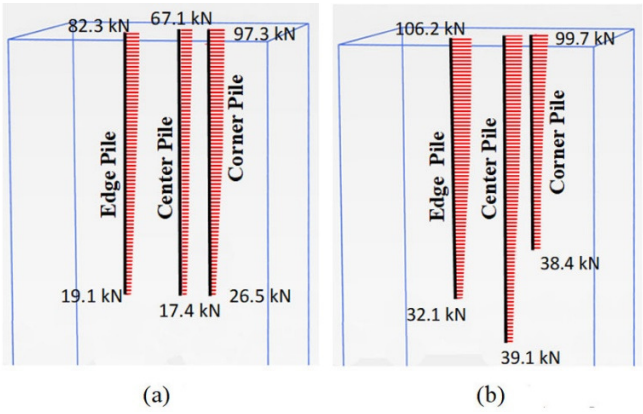


Fig. 8. Axial force (Nz) along the piles of the two pile groups.

## C. Result Comparison

The analysis of the field test indicates that, within the EL pile group at the point of collapsing failure, the load distribution on the head of Pile 1A surpasses that of Pile 1B by approximately 10% and that of Pile 1C by about 31%, signifying a notable disparity in load sharing within the group. Conversely, at the collapsing failure of the other pile group, the load on the head of Pile 2B exceeds that of Pile 2C by merely 5.5% and that of Pile 2A by roughly 8.4%. Besides, the load

borne by the edge piles (Pile 2B) in the VL pile group is approximately 17% greater than that supported by the corresponding Pile 1B in the EL pile group. This evidence suggests that variations in pile length not only increase the overall bearing capacity of the pile group but also improve the uniformity of load sharing among the individual piles (Figure 9).

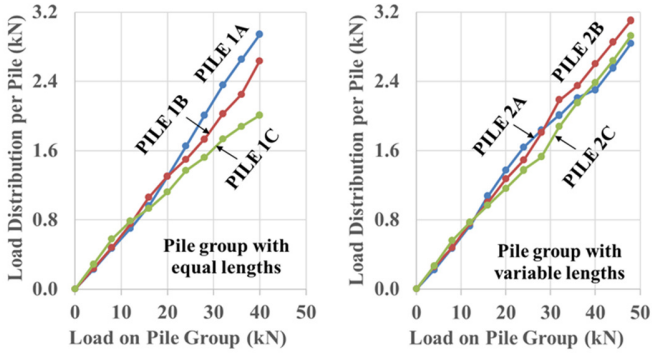


Fig. 9. Load distribution per pile top in the two pile groups (field test).

The FEM analysis provides an understanding of load distribution across each pile within two distinct pile groups. As illustrated in Figure 10, the load distribution in the EL pile group is uneven at the point of collapsing failure; specifically, the load borne by the top of the corner pile surpasses that of the edge pile by approximately 11.7% and exceeds that of the central pile by approximately 32.6%. Conversely, within the VL pile group, the load sharing on the edge pile is the greatest and the load distribution among the piles exhibits greater uniformity, with variations not exceeding 10%.

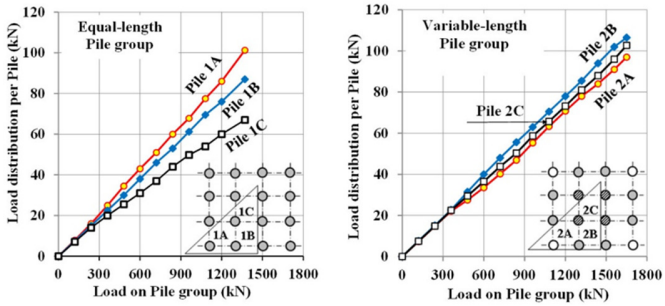


Fig. 10. Load distribution per pile of the two pile groups (FEM).

These comparisons show that, according to both methods, load distribution is more uniform in the VL pile group. In the field tests, the maximum difference of load sharing on the top of the pile in the EL group was about 31%. In contrast, in the VL group, the load difference among the piles did not exceed 10%. The FEM analysis confirmed these trends, showing that altering pile lengths within a group reduces load disparities and distributes axial forces more evenly.

Figure 11 presents the average unit shaft resistance as a function of displacement for both pile groups. Generally, when the displacements of the pile groups are minimal, the unit shaft resistances across all piles within each group are nearly identical. Displacements of approximately 12 mm are required to fully mobilize the shaft resistances of the tested piles. Within the EL pile group, the average unit-shaft resistance decreases sequentially as follows: corner pile (1A) 6.25 kPa, edge pile (1B) 5.5 kPa, and center pile (1C) 4.4 kPa. In the second pile group, the corresponding value diminishes in the order: edge pile (2B), corner pile (2A), and center pile (2C). The maximum values range from 6.4 kPa to 5.5 kPa.

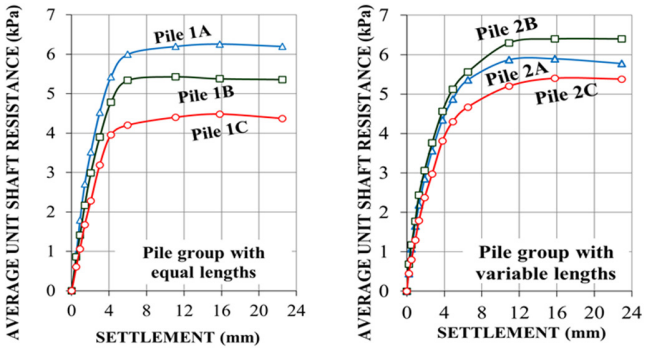


Fig. 11. Average unit shaft resistance - Settlement curves (field test)

In general, the unit shaft resistance measured by both studies exhibits similar trends (Figure 12). Within a pile group of equal length, the maximum average unit shaft resistances were approximately 4.7 kPa, 4.2 kPa, and 3.3 kPa for the corner, side, and center piles, respectively. Conversely, the corresponding values in the second group were noticeably higher and more uniform in comparison to those in the first group. The average unit shaft resistances obtained from FEM are marginally lower than the values obtained through field tests, potentially due to the resistance values increasing from top to bottom in accordance with the full-scale piles.

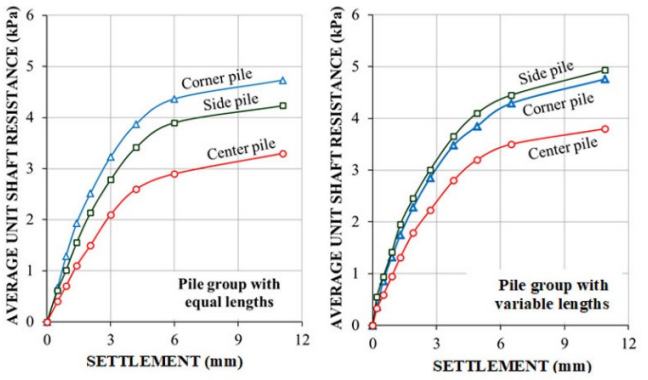


Fig. 12. Average unit shaft resistances – Settlement curves (FEM)

## IV. CONCLUSIONS

This study employs small-scale static load tests and the Finite Element Method (FEM) analysis to evaluate the performance of Equal-Length (EL) and Variable-Length (VL) pile groups with rigid caps under centric loading conditions. The primary conclusions derived from this investigation are:

- The VL pile group is an effective solution for centric load foundations. The results show that this pile group attains approximately 20% higher capacity and experiences a reduced 5% settlement compared to the EL pile group of identical size and total pile length.
- The load distribution within the EL pile group is uneven, with the load on the top of the corner pile being approximately 10% higher than that on the edge pile and 31% larger than that on the central pile. Conversely, the load distribution in another group has been improved; the differences in loads among the piles do not exceed 10%.
- The results of this study highlight the potential use of VL pile groups as a practical and economic method for foundation design. The quantitative analysis of these matters will be addressed in a subsequent paper.

## REFERENCES

[1] H. G. Poulos, "Piled raft foundations: design and applications," *Géotechnique*, vol. 51, no. 2, pp. 95–113, Mar. 2001, https://doi.org/10.1680/geot.2001.51.2.95.

[2] K. Watcharasawe, P. Jongpradist, P. Kitiyodom, and T. Matsumoto, "Measurements and analysis of load sharing between piles and raft in a pile foundation in clay," *Geomechanics and Engineering*, vol. 24, no. 6, pp. 559–572, Jan. 2021.

[3] C. V. Hoa and N. A. Tuan, "An analysis of raft thickness in high-rise buildings - case studies," *Strength of Materials and Theory of Structures*, no. 102, pp. 13–24, 2019.

[4] H. Cao Van and T. Nguyen Anh, "Establishing a Graphical Method for Calculation of Raft Thickness in Piled Raft, Pile Group and Raft Foundation," in *2020 3rd International Conference on Information and Computer Technologies (ICICT)*, San Jose, CA, USA, Mar. 2020, pp. 320–325, https://doi.org/10.1109/ICICT50521.2020.00056.

[5] S. Basack, S. Nimbalkar, and M. Zaman, "Recent developments in pile foundations: design, construction, innovations and case studies," *International Journal of Geotechnical Engineering*, vol. 17, no. 6, pp. 581–582, July 2023, https://doi.org/10.1080/19386362.2023.2380106.

[6] F. F. Chimdesa *et al.*, "Numerical analysis of pile group, piled raft, and footing using finite element software PLAXIS 2D and GEO5," *Scientific Reports*, vol. 13, Sept. 2023, Art. no. 15875, https://doi.org/10.1038/s41598-023-42783-x.

[7] R. M. S. Al-Ne'aimi and K. Q. Hussein, "Numerical Study of Pile Raft Foundation Behavior Under Vertical Loads and Large Moments," *Geotechnical and Geological Engineering*, vol. 42, pp. 97–119, 2024, https://doi.org/10.1007/s10706-023-02558-7.

[8] S. S. Gue, Y. C. Tan, and S. S. Liew, "Cost Effective Geotechnical Solutions For Roads And Factories Over Soft Ground," presented at the *20th Conference of the ASEAN Federation of Engineering Organization*, Phnom Penh, Cambodia, 2-5 Sept. 2002.

[9] Y. C. Tan, C. M. Chow, and S. S. Gue, "Piled raft with different pile length for medium-rise buildings on very soft clay," in *Proceedings of the 16th International Conference on Soil Mechanics and Geotechnical Engineering*, IOS Press, 2005, pp. 2045–2048.

[10] K. N. Kim, S.-H. Lee, K.-S. Kim, C.-K. Chung, M. M. Kim, and H. S. Lee, "Optimal pile arrangement for minimizing differential settlements in piled raft foundations," *Computers and Geotechnics*, vol. 28, no. 4, pp. 235–253, June 2001, https://doi.org/10.1016/S0266-352X(01)00002-7.

[11] C. V. Hoa, "Rational Pile Design using Computer-based Program Coding in Matlab: A Case Study," *Engineering, Technology & Applied Science Research*, vol. 14, no. 2, pp. 13160–13166, Apr. 2024, https://doi.org/10.48084/etasr.6867.

[12] H. V. Cao, T. A. Nguyen, and V. A. N. Le, "3D finite element analysis of the effect of raft thickness, pile spacing, and pile length on the behavior of piled raft foundation," *International Journal of GEOMATE*, vol. 23, no. 98, pp. 47–56, Oct. 2022, https://doi.org/10.21660/2022.98.3434.

[13] J. Feld, "Discussion on friction pile foundations," *Transactions of the American Society of Civil Engineers*, vol. 108, no. 1, pp. 73–115, 1943.

[14] *Standard Test Methods for Deep Foundations Under Static Axial Compressive Load*, ASTM D1143/D1143M-07, 2007.

[15] X. Dong, X. Tan, X. Lin, W. Guo, F. Zha, and L. Xu, "Reliability Analysis and Design of Vertically Loaded Piles in Spatially Variable Soils," *International Journal of Geomechanics*, vol. 23, no. 10, Oct. 2023, Art. no. 04023175, https://doi.org/10.1061/IJGNAI.GMENG-8426.

[16] K. Amornfa, H. T. Quang, and T. V. Tuan, "3D numerical analysis of piled raft foundation for Ho Chi Minh City subsoil conditions," *Geomechanics and Engineering*, vol. 29, no. 2, pp. 183–192, Jan. 2022.

[17] B. Asefa, E. Assefa, L. Pantelidis, and C. Sachpazis, "Pile configuration optimization on the design of combined piled raft foundations," *Modeling Earth Systems and Environment*, vol. 8, no. 3, pp. 3461–3472, Oct. 2022, https://doi.org/10.1007/s40808-021-01318-x.

[18] L. F. Sasso, A. C. Wagner, C. A. Ruver, L. da Silva Lopes, and N. C. Consoli, "Pile Groups and Piled Footings Bearing in Weakly Cemented Residual Soil," *Geotechnical and Geological Engineering*, vol. 41, no. 2, pp. 1485–1501, Mar. 2023, https://doi.org/10.1007/s10706-022-02349-6.